Non-growing *Rhodopseudomonas palustris* increases the hydrogen gas yield from acetate by shifting from the glyoxylate shunt to the tricarboxylic acid cycle

James B. McKinlay[1], Yasuhiro Oda[2], Martin Rühl[3], Amanda L. Posto[1], Uwe Sauer[3], and Caroline S. Harwood[2]

[1] Department of Biology, Indiana University, Bloomington, IN 47401
[2] Department of Microbiology, University of Washington, Seattle, WA 98195
[3] Institute of Molecular Systems Biology, ETH Zurich, Switzerland

*Running title: Electron distribution in H_2-producing non-growing cells

To whom correspondence should be addressed: James B. McKinlay, Tel: (812) 855-0359, Fax: (812) 855-6705, E-mail: jmckinla@indiana.edu

Keywords: Bacterial Metabolism, Biofuel, Nitrogenase, Metabolic engineering, Metabolic regulation, Metabolic tracers, Transcriptomics, Hydrogen Gas, Bacterial Starvation, Metabolic Flux Analysis

Background: The metabolism of non-growing microbes is poorly understood.
Results: In a nitrogen-starved and non-growing photoheterotrophic bacterium, metabolic flow was diverted to mobilize electrons for H_2 production.
Conclusion: During starvation bacteria decouple their metabolism from biosynthesis.
Significance: An understanding of metabolic activities of non-growing cells can be used to engineer improved biocatalysts.

ABSTRACT

When starved for nitrogen, non-growing cells of the photosynthetic bacterium *Rhodopseudomonas palustris* continue to metabolize acetate and produce H_2, an important industrial chemical and potential biofuel. The enzyme nitrogenase catalyzes H_2 formation. The highest H_2 yields are obtained when cells are deprived of N_2 and thus use available electrons to synthesize H_2 as the exclusive product of nitrogenase. To understand how *R. palustris* responds metabolically to increase H_2 yields when it is starved for N_2, and thus not growing, we tracked changes in biomass composition and global transcript levels. In addition to a 3.5-fold higher H_2 yield by non-growing cells we also observed an accumulation of polyhydroxybutyrate to over 30% of the dry cell weight. The transcriptome of *R. palustris* showed down-regulation of biosynthetic processes and up-regulation of nitrogen scavenging mechanisms in response to N_2 starvation but gene expression changes did not point to metabolic activities that could generate the reductant necessary to explain the high H_2 yield. We therefore tracked ^{13}C-labeled acetate through central metabolic pathways. We found that non-growing cells shifted their metabolism to use the tricarboxylic acid cycle to metabolize acetate in contrast to growing cells, which used the glyoxylate cycle exclusively. This shift enabled cells to more fully oxidize acetate, providing the necessary reducing power to explain the high H_2 yield.

INTRODUCTION

The vast majority of studies on microbial physiology and metabolism have been performed under conditions of nutrient excess. However, in most natural environments microbes are frequently starved for critical growth nutrients. While some mechanisms by which bacteria cope with starvation have been well characterized, such as cell differentiation and the stringent response, the diverse metabolic strategies employed by starving microbes is still poorly understood (1).

Purple nonsulfur bacteria, like *Rhodopseudomonas palustris*, are well known for their ability to grow photoheterotrophically, wherein light is used for energy and organic compounds are used for carbon and electrons. *R. palustris* will consume a variety of fermentation products, including acetate and volatile fatty acids (e.g., butyrate). When

growing, *R. palustris* metabolizes these compounds via acetyl-CoA and the glyoxylate shunt (2). The glyoxylate shunt bypasses the lower tricarboxylic acid (TCA) cycle, thereby retaining the two carbons in acetyl-CoA for biosynthesis that would otherwise be lost as CO_2. When starved for nutrients like nitrogen but supplied with light and organic carbon, *R. palustris* can maintain a relatively high rate of metabolic activity in a non-growing state for months or longer (3). Under these conditions, it is assumed that *R. palustris* repeatedly energizes and cycles electrons through a H^+-pumping electron transfer chain to generate ATP for cell maintenance in a process called cyclic photophosphorylation.

R. palustris has served as a model organism for studies of hydrogen gas (H_2) production (4). H_2 is an important chemical used in industries such as ammonia production and petroleum refining. It can also be used as a transportation fuel in H_2-powered vehicles. Nearly all H_2 currently used by our society is derived from fossil fuels. However, H_2 can be produced in a sustainable manner through a variety of methods, including biologically. *R. palustris* produces H_2 through the photosynthetic conversion of compounds that are abundant in agricultural waste, such as acetate. *R. palustris* makes H_2 via the enzyme, nitrogenase. Nitrogenase is best known for converting N_2 gas into NH_4^+ but H_2 is an additional obligate product of the reaction. If access to N_2 gas as a substrate is prevented, nitrogenase produces H_2 as its sole product. Most work has been done with cells expressing Mo-nitrogenase. *R. palustris* also encodes alternative iron (Fe-) and vanadium (V-) nitrogenases. These consume more reducing power and produce more H_2 per molecule of N_2 fixed than Mo-nitrogenase (5).

R. palustris regulatory mutants have been constructed that synthesize active nitrogenase and make H_2 while growing under an Ar atmosphere with NH_4^+ as the sole nitrogen source (2, 6–8). Under these growth conditions, the CO_2-fixing Calvin cycle competes with nitrogenase for electrons (2, 6). Genetically disrupting Calvin cycle activity increased the H_2 yield on all carbon sources tested (2). However, even the most electron-rich substrate tested, butyrate, gave a H_2 yield that was only 25% of the theoretical maximum as most of the electrons were used for biosynthesis. Thus, the main process that competes for electrons against H_2 production is biosynthesis. Indeed, when wild-type *R. palustris* growth was prevented by replacing N_2 with Ar, H_2 yields from acetate reached 43% of the theoretical maximum yield (9). This high H_2 yield and the ability to remain metabolically active for long periods of time makes starving *R. palustris* intriguing from both applied and fundamental perspectives.

Here we set out to understand the physiology of non-growing *R. palustris* cells that were starved for nitrogen, since it is under these conditions that the highest H_2 yields are observed. Excreted products, biomass composition, and global transcript abundances were monitored as *R. palustris* transitioned to and remained in a non-growing state. ^{13}C-tracer studies were performed to identify the central metabolic pathways that provide reductant for H_2 production. Together, these data inform on microbial responses to nitrogen starvation and provide a basis for engineering strategies to improve H_2 production traits.

EXPERIMENTAL PROCEDURES

Chemicals, strains, and culture and suspension conditions. Sodium [1-^{13}C]acetate and [U-^{13}C]acetate were purchased from Cambridge Isotope Laboratories (Andover, MA). *R. palustris* wild-type strain CGA009 was used for all experiments. CGA009 is defective in uptake hydrogenase activity (10). All cultures and suspensions were incubated at 30°C in front of 60W incandescent light bulbs. Strains were grown in a chemically defined medium, NFM (11), with N_2 gas as the sole nitrogen source in sealed, anaerobic 160 ml serum vials that were stirred with stir bars or in 27 ml anaerobic tubes. We generated suspensions of non-growing cells by flushing mid-exponential phase cultures (0.4-0.5 OD_{660}) with Ar for 10 min while stirring, thereby replacing the N_2.

Determining biomass composition. Cells were grown in 60 ml NFM with 20 mM unlabeled acetate. Duplicate vials of cell suspensions were chilled on ice at 0, 12, 30, 50, 90, 140, and 180 h of nitrogen starvation, and fractioned to quantify optical density, soluble compounds (e.g., acetate,

α-ketoglutartate [αKG]), gasses, and biomass components. Acetate and αKG were quantified by HPLC as described (12). H_2 and CO_2 were quantified by GC as described (6, 9). Total cell protein was quantified by the bicinchoninic acid assay (Thermo Fisher Scientific, Rockford, IL) as described (6). Dry cell weights (DCW) were determined as described (13) by filtering 25-ml of cell suspension through 0.22-micron PVDF filters (Millipore, Billerica, MA). Polyhydroxybutyrate (PHB) was then hydrolyzed and extracted as crotonic acid by boiling the filters and cells in 1 ml pure sulfuric acid in screw-cap glass test tubes. Extracts were diluted with 4 ml water, centrifuged, filtered, and diluted 10-fold with water. Crotonic acid was quantified by HPLC as described (14). Total RNA and glycogen were quantified from 5 ml of cell suspension as described (13) except a glucose oxidase assay kit (Sigma, St. Louis, MO) was used to quantify glucose from glycogen. Trehalose was quantified by centrifuging 5 ml of cell suspension, resuspending in 0.4 ml of 50 mM sodium acetate buffer (pH 5.2), lysing cells by sonication, boiling for 5 minutes, incubating with 0.04 U of trehalase (Sigma) for 20 h at 37ºC, diluting with 0.4 ml of 250 mM Tris-HCl (pH 7.5), and then quantifying the resulting glucose using a glucose oxidase assay kit. Fatty acids were quantified as methyl esters from ~ 7 ml of cell suspension as described (15) using a Shimadzu GC-2014 with a 15 m SHRXI-5MS column (Columbia, MD). The electron content of biomass excluding PHB was determined from OD_{660} values at the onset of starvation using an experimentally determined conversion factor for growing cells of 625 mg DCW L^{-1} OD_{660}^{-1} and a biomass molecular formula of $CH_{1.8}N_{0.18}O_{0.38}$ (16), which would yield 5 available electrons per carbon. An increase in biomass electron content of 1.2 was then applied based on the average increase in colony forming units after starvation (see Results).

RNA-seq using R. palustris*-specific selective primers*. RNA was extracted and purified from 5 ml of the same cell suspensions and time points used for tracking the biomass composition, as described previously (17). The *R. palustris*-specific selective primers v2 were based on the genome sequences of six *R. palustris* strains (CGA009, TIE-1, HaA2, BisB5, BisB18, and BisA53). We used a pool of 1,203 selective primers with no perfect match to any rRNA genes (e.g., 5S, 16S, and 23S rRNA). An additional set of 200 primers that were responsible for the majority of rRNA-priming events in test libraries, was further removed, leaving a final set of 1,003 *R. palustris*-specific selective primers v2 (Table S1). For first strand cDNA synthesis, 500 ng of total RNA was mixed with 1 µl of 100 µM of *R. palustris*-specific selective primers v2 in 5 µl reaction volume, and incubated at 65 °C for 5 min. After snap chilling on ice, 2 µl of 5X First-Strand Buffer (Invitrogen, Carlsbad, CA), 2 µl of 10 mM dNTP mix (New England BioLabs, Ipswich, MA), 0.5 µl of 0.1 M DTT, 0.5 µl of SuperScript III Reverse Transcriptase (Invitrogen) were added, and the mixture was further incubated at 40°C for 90 min. To generate the second strand, 45.5 µl of water, 15 µl of 5X Second Strand Buffer (Invitrogen), 1.5 µl of 10 mM dNTP mix, 0.5 µl of *Escherichia coli* DNA Ligase (Invitrogen, 10 U/µl), 2 µl of DNA Polymerase I (Invitrogen, 10 U/µl), and 0.5 µl of RNase H (Invitrogen, 2 U/µl) were added to the reaction, and incubated at 16 °C for 2 h. The reaction was stopped by adding 25 µl of 20 mM EDTA, pH 8.0. Double stranded cDNA was then purified by using the MinElute PCR Purification Kit (QIAGEN, Valencia, CA) using 12 µl of Buffer EB. Finally, the cDNA library was constructed using the Ovation Ultralow DR Multiplex System (NuGEN, San Carlos, CA) following the manufacture's instructions. All cDNA libraries were sequenced with an Illumina HiSeq at the University of Washington High Throughput Genomics Center, and raw sequencing data were processed by with the Xpression pipeline (18). Reads that mapped to the reference genome sequence of *R. palustris* CGA009 were categorized as (i) uniquely mapped (aligned with $\leq$ 2 mismatches to a single genomic locus), (ii) partially mapped (aligned with > 2 mismatches or one gaps to a single genomic locus), (iii) non-uniquely mapped (aligned to the 5S, 16S, and 23S rRNA genes, or multiple genomic locus), and (iv) unmapped (no alignment to a reference genome). Only the uniquely mapped reads were subjected to further analysis. The number of reads overlapping each gene was recorded and normalized based on reads per kilobase per million uniquely mapped reads (RPKM). We used the statistical software DESeq (19) to evaluate whether, for a given region, an observed difference in read counts

between t_x and t_0 was significant. Features were considered to be differentially expressed from levels observed immediately prior to nitrogen starvation if they had a *p*-value of ≤0.001 and with fold change ratios ≥ 4. The resulting data has been deposited in NCBI's Gene Expression Omnibus (20) under the GEO Series accession number GSE51825.

Definition of the theoretical maximum H_2 yield. The maximum amount of H_2 that can be produced from electrons made available when an organic substrate is fully oxidized to CO_2. For example, the theoretical maximum H_2 yield from acetate is 4 moles H_2/mole acetate according to:

$$C_2H_4O_2 + 2H_2O \rightarrow 2CO_2 + 8H^+ + 8e^-$$
$$\underline{8H^+ + 8e^- \rightarrow 4H_2}$$
$$C_2H_4O_2 + 2H_2O \rightarrow 2CO_2 + 4H_2$$

^{13}C-Labeling experiments and mass spectrometry. One ml of 10 ml-starter cultures grown in NFM acetate were used to inoculate 50 ml of NFM with 10 mM unlabeled acetate in 160 ml anaerobic serum vials with an N_2 headspace. When a cell density of 0.4-0.5 OD_{660} was reached the headspace was replaced with Ar to halt growth and cells were incubated for ~100 h during which time PHB accumulated. Suspensions were then decanted into 50 ml conical tubes in an anaerobic chamber, centrifuged, washed once with anaerobic phosphate buffer (12.5 mM NaH_2PO_4, 12.5mM K_2HPO_4), resuspended in 1 ml of phosphate buffer, and then transferred into anaerobic 160-ml serum vials containing 56 ml of NFM with 10 mM of either [1-^{13}C]acetate (three biological replicates), [U-^{13}C]acetate (1 cell suspension), or unlabeled acetate (4 biological replicates). Cell suspensions were then flushed with Ar for 10 min while stirring. Unlabeled cell suspensions were then sampled and later harvested (260 h after receiving ^{13}C-acetate; 360 h after starvation was initiated) to determine the changes in acetate, αKG, CO_2, H_2 and PHB. Labeled cell suspensions were sampled periodically (~every two days) to track optical densities, acetate consumption, and H_2 production before being quenched. Individual cell suspensions were quenched 215, 260, and 283 h after receiving ^{13}C-acetate (316, 360, and 384 h of starvation; the suspension with [U-^{13}C]acetate was harvested after 316 h of starvation). Cell suspensions were quenched as described (19) by decanting cell suspensions into 200 ml of 60% methanol with 10 mM ammonium acetate (pH 7.2) at -40°C. Quenched suspensions were centrifuged at 14,300 rcf in a rotor pre-chilled to -20°C. Quenched samples were not pooled (21). The supernatant was discarded and the remaining cell pellet was frozen in liquid N_2 and stored at -80°C until the extraction procedure. Metabolites were extracted from cell pellets three times with 78°C ethanol as described (21), dried under N_2 at 55°C, and then were stored at -80°C. Samples were resuspended in water and the metabolites analyzed by LC-MS/MS as described (21). Despite the larger culture volumes, we only observed a portion of those metabolites and fragments that were observed using the same methods on nitrogen-starved *B. subtilis* (21). Even so, we observed sufficient metabolite labeling patterns to resolve key fluxes in the *R. palustris* metabolic network and with enough redundancy to perform statistical analyses.

^{13}C-Metabolic flux analysis. Flux values were estimated from the measured acetate uptake rate and carbon product formation rates and from metabolite mass isotopomer distributions using the software suite, 13CFLUX2 (www.13cflux.net/13cflux2/index.jsp) (22). Data from the single [U-^{13}C]acetate-labeled culture were included as additional constraints using a relatively large SD (0.025) for each mass isotopomer to put more weight on the data from [1-^{13}C]acetate-labeled cultures. The average SD for all mass isotopomers from the [1-^{13}C]acetate-labeled cultures was 0.015. All mass isotopomer data were fit against a single metabolic model as described (23). The metabolic model was based on that previously described for *R. palustris* (6), but excluded biosynthetic outputs, included αKG, PHB, and glycogen outputs, and included inputs of unlabeled metabolites from biomass degradation pathways. Various modifications of this model were explored as described in the results (e.g., omitting malic enzyme, constraining malate dehydrogenase directionality). For the final model the fitting algorithm was initiated using 1300 different arrangements of starting values chosen at random using the 13CFLUX2 program, *multifit*. The fitting algorithm was applied to other models using at least 300 different starting value

arrangements. Standard deviations for flux values were determined using the 13CFLUX2 linearized statistical analysis program, *fwdsim*.

RESULTS

Electron flow during nitrogen starvation. *R. palustris* was grown anaerobically in mineral medium with N_2 gas as the sole nitrogen source and acetate as the carbon source. Light was provided as the energy source. When cells reached the mid-logarithmic phase of growth, we removed the N_2 by flushing the headspace of the sealed growth vessels with Ar. Entire cultures were then harvested for analysis of excreted products, biomass composition, and global transcript levels at various intervals for a week (180h) following the initiation of nitrogen starvation. Starved cells consumed acetate and produced hydrogen and CO_2 (Fig 1). These non-growing cells also produced αKG, as reported previously (9). H_2 production was most rapid at the beginning of the experiment then declined considerably after 100 hours (Fig 1). Similar trends and timing were observed for CO_2 production and acetate consumption (Fig 1). As the production of H_2 and CO_2 declined, the rate of αKG production increased after 50 h (Fig 1). Similar to previous observations (9), H_2 and αKG together accounted for about half of the electrons consumed (H_2: 45 ± 5% and αKG: 1.7 ± 1.6%; SD; n=11; across time points from 12h - 180h). Including cell suspensions from other experiments, the H_2 yield was sometimes observed to exceed 50% of the theoretical maximum yield (6 out of 16 suspensions), reaching 66% in one case.

We hypothesized that the remaining electrons could have been incorporated into internal storage products. The genome sequence of *R. palustris* (24) suggests that it can make several different storage products including glycogen, trehalose, and PHB. We found that, there was a large accumulation of PHB upon nitrogen starvation (Fig. 2). Before starvation, no PHB was detected. Upon starvation, PHB accumulated and eventually accounted for over 30% of the DCW and 35 ± 6% of the electrons consumed. PHB accumulation followed a similar trend to that of acetate consumption and H_2 and CO_2 production, with the most rapid production occurring in the first 50 h of starvation. Glycogen and trehalose showed a brief accumulation after starvation began, but levels never accounted for more than 2% of the DCW (Fig. 2). Protein, RNA, and lipids showed less dramatic fluctuations in response to starvation (Fig. 2), although the phospholipid fatty acid composition changed. There was an overall shift from unsaturated fatty acid to saturated fatty acids and cyclopropane fatty acids. C18:1 fatty acids decreased from 75% to 59% of the total fatty acid composition by 180h of starvation while C16:0 fatty acids increased from 10% to 20% (Fig. 3a). This decrease in C18 fatty acids could have contributed acetyl-CoA to central metabolism and perhaps to the synthesis of C20:0 fatty acids which accumulated to nearly 2% of the cellular fatty acids by 180h (Fig. 3b). Nitrogen-starved cells also produced C17 and C19 cyclopropane fatty acids, together accounting for 5-6% of the fatty acid composition by 180h (Fig. 3b).

We also took into account electrons used to make new cells after nitrogen starvation. Surprisingly, the OD of cultures increased 2.0 ± 0.1-fold (SD; n = 6) after removing N_2. However, this OD increase was not simply due to cell division. Colony forming unit counts indicated that cell numbers only increased 1.2 ± 0.1-fold (SD; n = 4). We determined that the large OD increase was due to PHB accumulation. A mutant of *R. palustris* that is incapable of PHB synthesis (Oda, McKinlay, and Harwood; unpublished) only showed a 1.2 ± 0.2-fold (SD; n = 4) increase in OD upon nitrogen starvation. This brief increase in biomass was estimated to account for 25 ± 5% of the electrons consumed.

Taken together we determined that electrons from consumed acetate are distributed between H_2, αKG, PHB, and a 1.2-fold increase in cells. These products account for 106 ± 12% (SD; n=11; across time points from 12h - 180h) of the electrons consumed. The carbon balance, including measurements of CO_2, shows that 99 ± 15% (SD; n=11) of the acetate carbon consumed is accounted for in these products. Thus we identified all major endpoints of electron flow from acetate during nitrogen starvation.

Transcriptome analysis did not reveal significant metabolic changes. We also isolated RNA from cells at the same time points as above to analyze the transcriptome of nitrogen-starved

cells (Table S2). General trends that emerged were (i) up-regulation of genes involved in scavenging nitrogen, (e.g., the V- and Fe-nitrogenases) and (ii) down-regulation of core house-keeping and biosynthetic genes (e.g., ribosomal proteins, photosynthetic proteins) (Fig. 4).

The transcriptomic dataset may also provide insight into the observed metabolic and cell composition changes noted above. RPA0895 and RPA2160, which encode 3-oxoacyl-ACP reductases, could be involved in the shift towards unsaturated fatty acids (Table S2). These genes were upregulated in response to nitrogen starvation in contrast to most other genes involved in fatty acid synthesis (e.g., those encoding acetyl-CoA carboxylase; RPA0508, 2435-6; Table S2). Most notably RPA2160 transcript levels increased >60-fold by 180h. RPA3082 was the only one of three potential cyclopropane-fatty-acyl-phospholipid synthase genes (RPA0924, 2569, 3082) that showed significantly higher transcript levels (Table S2), especially from 90h onwards, coinciding with the increase in cyclopropane fatty acids.

Transcript levels for core metabolic processes such as ATPase (RPA0175-9 and RPA0843-7), NADH-ubiquinone dehydrogenase (RPA4252-64), and transhydrogenase (RPA4181-2) decreased upon nitrogen starvation (Table S2). Figure 4F illustrates that most genes encoding central metabolic enzymes exhibited either lower transcript levels or no differential expression. The only two central metabolic genes that showed consistently higher transcript levels were RPA1329, encoding one of two fumarases, and RPA1331, encoding malate quinone oxidoreductase, although p-values were above the threshold for all time points (Table S2). These lower transcript levels for metabolic genes are consistent with the slower metabolism of nitrogen-starved cells. The acetate uptake rate (which dictates an upper-limit for all downstream flux values) by non-growing cells in this study was 0.042 ± 0.007 μmol mg DCW^{-1} h^{-1} whereas growing cells consumed acetate at 2.0 ± 0.0 μmol mg DCW^{-1} h^{-1} (6).

Although there was some consistency between transcriptomic and physiological data it was clear that the transcriptomic data did not provide a complete picture of the physiological response to nitrogen starvation. For example, genes potentially involved in PHB synthesis (acetyl-CoA acetyltransferases, RPA0513, 175 and 3715; 3-hydroxybutyrl-CoA dehydrogenase, RPA4748; and PHB synthase, RPA2501) did not show significant transcript level changes (Table S2) despite prolific PHB accumulation. If not for the PHB measurements, one might misinterpret the transcriptomic dataset to indicate PHB degradation. A potential PHB depolymerase gene, RPA0565 showed up to 5-fold higher transcript levels in response to nitrogen starvation (Table S2).

More importantly, the transcriptomic data did not indicate how reductant was generated to explain the high H_2 yields. Previously we determined that an *R. palustris* Calvin cycle mutant growing on acetate uses half of its reducing power to produce H_2 at about 14.5% of theoretical maximum yield and the other half for biosynthesis (6). Thus, if biosynthesis were prevented, we would only expect there to be enough reducing power diverted from biosynthesis to produce H_2 at 29% of theoretical maximum yield. However, we observed that nitrogen-starved cells produce H_2 at levels up to 66% of the theoretical maximum yield. Thus, additional reducing power must be generated in nitrogen-starved cells. To determine how this additional reducing power was generated we turned to ^{13}C-labeling experiments.

Nitrogen-starvation causes a shift in metabolic flux from the glyoxylate shunt to the TCA cycle. Distribution of metabolic fluxes at branch points can be inferred from the unique patterns of ^{12}C and ^{13}C that each branch will produce when an organism is fed a ^{13}C-labeled substrate (25). We previously used such techniques to determine metabolic fluxes during photoheterotrophic growth using the labeling patterns in proteinaceous amino acids (2, 6). However, nitrogen-starved cells do not synthesize amino acids and protein at a sufficient level for this approach. Thus, we examined the labeling patterns in the organic acids and sugar phosphates of central metabolism (21). We initiated these experiments with cells that had already been subjected to 100 h of nitrogen starvation, and thus were synthesizing little PHB,

prior to receiving either [1-^{13}C]acetate or [U-^{13}C]acetate. We chose to incubate cells with ^{13}C-acetate after the PHB accumulation phase to avoid any possible metabolic changes during this transition that could impact labeling patterns.

The first major branchpoint during the metabolism of acetate in *R. palustris* is the split to the glyoxylate shunt versus the lower tricarboxylic acid (TCA) cycle at isocitrate. The flux distribution at this branchpoint could have a large influence on reductant availability since the lower TCA cycle generates two reducing equivalents (e.g., 2 NAD(P)H) whereas the glyoxylate shunt does not generate any. The glyoxylate shunt flux would result in double-labeled succinate, malate and αKG from [1-^{13}C]acetate whereas TCA cycle flux would result in single-labeled succinate and malate and a mixture of single and double-labeled αKG (Fig 5). A high proportion of succinate (82.5%) was single-labeled while only a small percentage (4.9%) was double-labeled (Fig.5) strongly indicating a large TCA cycle flux with very little participation from the glyoxylate shunt. High proportions of both single- and double-labeled αKG (inferred from measurements of free glutamate) also indicate a high TCA cycle flux (Fig. 5). On its own, the high proportion of double-labeled malate (~37%) suggests a large involvement from the glyoxylate shunt. However, even double-labeled malate can only give rise to single labeled succinate through the action of the TCA cycle (Fig. 5). Thus, a pathway other than the glyoxylate shunt must have generated the double-labeled malate.

We then examined the complete mass isotopomer data set using 13CFLUX2 for two reasons: (i) to look for other activities that could generate the double-labeled malate while taking into account the labeling patterns observed in other metabolites and (ii) to quantify metabolic fluxes and thereby the contribution of the TCA cycle towards H_2 production. The equations used to determine metabolic fluxes from labeling patterns describe both an isotopic and metabolic steady state (which can be satisfied by a pseudo-metabolic steady state in batch culture). Cell suspensions were harvested at different time points so that we could confirm isotopic steady state by comparing the mass isotopomer distributions (MIDs). Most of the MIDs from the three [1-^{13}C]acetate-fed cultures were similar across time points (individual mass isotopomers showed SD ≤ 10% of the mean), indicating an isotopic steady state. There are a few mass isotopomers that showed a larger variation across time points that may have influenced the determination of flux values (4 out of 42 mass isotopomers had a SD between 10 and 16% of the mean). However, there are enough redundant measurements to provide confidence in our main conclusions. Suspensions were harvested after the PHB accumulation phase to avoid a possible metabolic shift occurring at this time. After PHB accumulation, we also observed constant rates of acetate consumption and H_2 production up to 384 h indicating a pseudo-metabolic steady state.

To look for pathways that could explain the double-labeled malate, we started with the metabolic model depicted in Figure 6. This model also takes into the account the possibility of metabolites entering central metabolism from the degradation of unlabeled biomass macromolecules. Arbitrary flux values were repeatedly optimized to generate a simulated data set that fit the experimentally determined MIDs and product formation rates (i.e., CO_2, αKG, and PHB). The best flux solutions (i.e., that resulted in a minimal difference between the simulated and measured data sets) indicated massive cycling between malate, pyruvate, PEP, and oxaloacetate in either direction (Fig. 7a). This cycling would result in the exchange of an unlabeled carboxyl with $^{13}CO_2$ (Fig 7a; $^{13}CO_2$ is the dominant form of CO_2 in the cell suspensions since it is derived from the labeled-carboxyl of [1-^{13}C]acetate). To explore other possibilities, we then ran the fitting algorithm using a model lacking malic enzyme (malate → pyruvate + CO_2) to prevent the cycling noted above. An equally good solution was reached in which the double-labeled malate was explained by a high decarboxylating/carboxylating exchange flux between malate and PEP, involving malate dehydrogenase (Fig. 7b). When both the malic enzyme reaction and malate dehydrogenase exchange flux were removed from the model, malate patterns could still be largely explained by gluconeogenic exchange fluxes producing malate from patterns generated in the non-oxidative pentose phosphate pathway. Thus, there are several solutions that can explain the double-

labeled malate. Importantly, none of these solutions involved the glyoxylate shunt as this activity would also generate double-labeled succinate.

Unlike the multiple flux solutions that could explain the double-labeled malate, all the tested models consistently showed a nearly exclusive involvement of the lower TCA cycle relative to the glyoxylate shunt. This trend is in stark contrast to the nearly exclusive use of the glyoxylate shunt observed in growing cells (Fig. 6). The reducing power from the high TCA cycle flux was enough to fully explain the large H_2 yield (Fig. 8). Other potential sources of reducing power, such as the oxidative pentose phosphate pathway exhibited negligible flux (Fig. 6). While we are not confident in all aspects of the flux map (Fig. 6; gray arrows), we note that the final solution balanced electrons to within 97% (Fig. 8), even though electron balance was not a constraint used by the fitting algorithm.

Discussion

Here we determined that when *R. palustris* growth is prevented by nitrogen starvation, acetate is metabolized through the TCA cycle rather than through the glyoxylate shunt. This TCA cycle flux results in a higher production of CO_2 and reducing power than in growing cells (Fig. 6). The reducing power must be oxidized to maintain metabolic flow. Oxidation of reducing power is primarily coupled to H_2 production, resulting in a 3.5-fold increase in H_2 yield over growing cells (Fig. 8). It is currently not clear why the H_2 production slowed to a third of the initial rate after 50-100 h of starvation (Fig. 1). It is unlikely that the slow rate was due to inhibition of nitrogenase by accumulated H_2 because resuspending cells in fresh medium under Ar after 100 h (i.e., for ^{13}C-labeling experiments) did not restore the early rapid H_2 production typically observed upon nitrogen starvation (Fig. 1). The slow H_2 production rate is tied to a slower rate of metabolism overall, as acetate uptake and CO_2 production also slowed (Fig. 1). We speculate that *R. palustris* might first respond to limiting nitrogen by rapidly filling up its PHB carbon stores and then switch to a lower metabolic rate. The highest PHB level we observed (~ 30% DCW) may represent a physiological maximum as it is an order of magnitude above levels typically reported for growing cells (26) and comparable to one of the highest values reported for *R. palustris* (27).

The large increase in electron-rich PHB in the first few days of starvation (Fig. 2) is also likely an important electron sink that was not reflected in our flux maps (Fig. 6 and 8) because we conducted ^{13}C-labeling experiments after PHB synthesis had slowed. PHB synthesis is a known response to nitrogen limitation in *R. palustris* (28) and other bacteria (29). PHB was also synthesized when *R. palustris* and other purple non-sulfur bacteria were starved for phosphorous (26) or sulfur (30), but under these conditions PHB synthesis was greatly favored over H_2 production. *R. palustris* also produced cyclopropane fatty acids when starved for nitrogen. Although the role of these fatty acids is unclear in bacteria, they are usually made in response to stressors (e.g., acid shock in *E. coli* (31)) and may be involved in coordinating stress responses. For example, a potential cyclopropane fatty acid synthase was shown to be needed for the proper transcriptional activation of a stress response to singlet oxygen in *Rhodobacter sphaeroides* (32).

The most notable discovery from our study was the metabolism of acetate via the TCA cycle instead of via the glyoxylate shunt. The glyoxylate shunt is canonically employed during growth on acetate to bypass the lower TCA cycle, which would otherwise result in the loss of the two acetate carbons as CO_2. Lesser known, the glyoxylate shunt is also activated in bacteria such as *E. coli* during growth on glucose, for example to prevent unnecessary carbon loss via the TCA cycle when glucose is limiting or to prevent excess production of reducing power via the TCA cycle when other oxidative pathway fluxes are high (33). A few studies have followed the metabolism of ^{13}C-labeled acetate in growing cells. During aerobic respiration on acetate by *Corynebacterium glutamicum*, 25% of isocitrate was metabolized via the glyoxylate shunt while 75% was diverted through the lower TCA cycle (34). It was speculated that the relatively high *C. glutamicum* TCA cycle fluxes were needed to generate sufficient reductant for respiration to support the high ATP demands of gluconeogenesis. Similar

results were observed in *E. coli* respiring with acetate, with 30% of flux from isocitrate going to the glyoxylate shunt and 70% through the lower TCA cycle (35). A ^{13}C-labeling study of *Geobacter metallireducens* showed high TCA cycle flux from acetate while respiring with Fe^{3+} with zero flux through the glyoxylate shunt (36). However, this depiction was misleading as there is nothing in the genome sequence to suggest that the glyoxylate shunt exists in *G. metallireducens* and rather pyruvate synthase is likely critical to assimilate acetate. The high reductant demand of respiration is not an issue for *R. palustris* under photosynthetic conditions. Indeed when we grew *R. palustris* photosynthetically with ^{13}C-acetate we observed a nearly complete absence of TCA cycle flux with acetate metabolized almost exclusively via the glyoxylate shunt (6). When *R. palustris* is starved for nitrogen, we conclude that there are few remaining sinks for carbon in the absence of biosynthesis and with PHB already accumulated. Thus instead of conserving carbon via the glyoxylate shunt the TCA cycle is activated to oxidize acetate to CO_2. Oxidation of carbon sources to CO_2 may be a widespread bacterial response to nitrogen deprivation, even in non-photosynthetic, respiring bacteria. ^{13}C-metabolic flux analysis of nitrogen-starved *B. subtilis* fed with glucose also showed elevated fluxes through CO_2-producing oxidative pathways (37).

The transcriptomic data informed on several physiological aspects of the starving cells. The increase in transcript levels for nitrogen scavenging genes is consistent with previous microarray observations of *R. palustris* strains during growth with inefficient nitrogenase isozymes that likely induced a state of nitrogen starvation (5). The decrease in transcript levels for genes encoding biosynthetic and central metabolic enzymes is also consistent with expectations for non-growing cells. For example, transcript and protein levels were shown to decrease with decreasing growth rate in *E. coli* (38). However, we also observed instances where metabolic shifts could not have been predicted from the transcriptomic dataset – namely PHB synthesis and the branching of flux through the glyoxylate shunt and TCA cycle.

Transcripts for PHB synthesis genes were not differentially regulated despite PHB accumulation. This observation suggests that these genes are constitutively expressed and thus are regulated post-transcriptionally, similar to reports for other bacteria (29, 39). The surprising increase in expression of PHB depolymerase despite PHB accumulation may be indicative of simultaneous PHB synthesis and degradation. These concurrent opposing activities have been noted in other bacteria and can allow for PHB to be remodeled into other polyhydroxyalkanoates (29).

The glyoxylate shunt isocitrate lyase gene can be transcriptionally regulated in *R. palustris*. Transcript levels were 11-fold lower during growth on succinate (which does not require the glyoxylate shunt), compared to growth on acetate (based on microarray data comparison between GPL3954 [GSM798294 and GSM798299] and GSE5194 [GSM116900 and GSM116886]; data accessible in the NCBI GEO database (20)). However, during nitrogen starvation we did not observe such a decrease in isocitrate lyase transcript levels despite the low glyoxylate shunt flux (Fig. 4F). Thus, the shift of flux from the glyoxylate shunt to the TCA cycle must not be transcriptionally regulated under these conditions. The TCA cycle enzyme, isocitrate dehydrogenase has a higher affinity for isocitrate (Km: 0.009mM (40)) than isocitrate lyase does (Km: 0.136 mM (41)) and thus could simply outcompete isocitrate lyase for isocitrate. In *E. coli*, isocitrate dehydrogenase activity is also inhibited by phosphorylation of the enzyme (42). If similar post-translational regulation is used in *R. palustris* then we can infer that isocitrate dehydrogenase is primarily in an unphosphorylated state during nitrogen starvation. However, biochemical or proteomic analyses would have to be performed to confirm that both enzymes are present and able to compete for isocitrate.

The discrepancies between our transcriptomic and fluxomic data demonstrate the need for cautious interpretations of metabolic trends from transcriptomic datasets. Our data and that obtained from nitrogen-starved *B. subtilis* (37), demonstrate that bacteria can have low transcript levels for metabolic genes and yet remain metabolically active. In the case of *R. palustris*, metabolic

activity can persist in the absence of growth for months (3). This metabolic activity during starvation involved a constant input of energy (light) and electrons (acetate). Thus it is not clear whether our results can be extended to suggest that 'dormant' microbes that exhibit little to no detectable rRNA in natural environments may still contribute metabolic activity to a community (43). However, conditions of constant energy, carbon, and electron inputs under otherwise growth-limiting conditions is certainly relevant to industrial bioprocesses where starvation is used to favor product formation over biosynthesis. Thus, newly configured tools for directly analyzing the metabolism of starving cells (37) will be crucial to understand and optimize their industrial attributes.

References

1. Lennon, J. T., and Jones, S. E. (2011) Microbial seed banks: the ecological and evolutionary implications of dormancy. *Nat. Rev. Microbiol.* **9**, 119–30

2. McKinlay, J. B., and Harwood, C. S. (2011) Calvin cycle flux, pathway constraints, and substrate oxidation state together determine the H2 biofuel yield in photoheterotrophic bacteria. *MBio* **2**, 10.1128/mBio.00323–10

3. Gosse, J. L., Engel, B. J., Hui, J. C., Harwood, C. S., and Flickinger, M. C. (2010) Progress toward a biomimetic leaf: 4,000 h of hydrogen production by coating-stabilized nongrowing photosynthetic *Rhodopseudomonas palustris*. *Biotechnol. Prog.* **26**, 907–918

4. McKinlay, J. B., and Harwood, C. S. (2010) Photobiological production of hydrogen gas as a biofuel. *Curr. Opin. Biotechnol.* **21**, 244–251

5. Oda, Y., Samanta, S. K., Rey, F. E., Wu, L., Liu, X., Yan, T., Zhou, J., and Harwood, C. S. (2005) Functional genomic analysis of three nitrogenase isozymes in the photosynthetic bacterium *Rhodopseudomonas palustris*. *J. Bacteriol.* **187**, 7784–7794

6. McKinlay, J. B., and Harwood, C. S. (2010) Carbon dioxide fixation as a central redox cofactor recycling mechanism in bacteria. *Proc. Natl. Acad. Sci. U S A* **107**, 11669–11675

7. Rey, F. E., Heiniger, E. K., and Harwood, C. S. (2007) Redirection of metabolism for biological hydrogen production. *Appl. Environ. Microbiol.* **73**, 1665–1671

8. Adessi, A., McKinlay, J. B., Harwood, C. S., and De Philippis, R. (2012) A *Rhodopseudomonas palustris nifA** mutant produces H_2 from NH_4^+-containing vegetable wastes. *Int. J. Hydrog. Energy* **37**, 15893–15900

9. Huang, J. J., Heiniger, E. K., McKinlay, J. B., and Harwood, C. S. (2010) Production of hydrogen gas from light and the inorganic electron donor thiosulfate by *Rhodopseudomonas palustris*. *Appl. Environ. Microbiol.* **76**, 7717–7722

10. Rey, F. E., Oda, Y., and Harwood, C. S. (2006) Regulation of uptake hydrogenase and effects of hydrogen utilization on gene expression in *Rhodopseudomonas palustris*. *J. Bacteriol.* **188**, 6143–6152

11. Kim, M., and Harwood, C. S. (1991) Regulation of benzoate-CoA ligase in *Rhodopseudomonas palustris*. *FEMS Micrbiol Lett* **83**, 199–203

12. McKinlay, J. B., Zeikus, J. G., and Vieille, C. (2005) Insights into *Actinobacillus succinogenes* fermentative metabolism in a chemically defined growth medium. *Appl. Environ. Microbiol.* **71**, 6651–6656

13. McKinlay, J. B., Shachar-Hill, Y., Zeikus, J. G., and Vieille, C. (2007) Determining *Actinobacillus succinogenes* metabolic pathways and fluxes by NMR and GC-MS analyses of ^{13}C-labeled metabolic product isotopomers. *Metab. Eng.* **9**, 177–192

14. Karr, D. B., Waters, J. K., and Emerich, D. W. (1983) Analysis of poly-3-hydroxybutyrate in *Rhizobium japonicum* bacteroids by ion-exclusion high-pressure liquid chromatography and UV detection. *Appl. Environ. Microbiol.* **46**, 1339–1344

15. Li, Y., Beisson, F., Pollard, M., and Ohlrogge, J. (2006) Oil content of Arabidopsis seeds: The influence of seed anatomy, light and plant-to-plant variation. *Phytochemistry* **67**, 904–915

16. Carlozzi, P., and Sacchi, A. (2001) Biomass production and studies on *Rhodopseudomonas palustris* grown in an outdoor, temperature controlled, underwater tubular photobioreactor. *J. Biotechnol.* **88**, 239–49

17. Hirakawa, H., Oda, Y., Phattarasukol, S., Armour, C. D., Castle, J. C., Raymond, C. K., Lappala, C. R., Schaefer, A. L., Harwood, C. S., and Greenberg, E. P. (2011) Activity of the *Rhodopseudomonas palustris* p-coumaroyl-homoserine lactone-responsive transcription factor RpaR. *J. Bacteriol.* **193**, 2598–2607

18. Phattarasukol, S., Radey, M. C., Lappala, C. R., Oda, Y., Hirakawa, H., Brittnacher, M. J., and Harwood, C. S. (2012) Identification of a p-coumarate degradation regulon in *Rhodopseudomonas palustris* by Xpression, an integrated tool for prokaryotic RNA-seq data processing. *Appl. Environ. Microbiol.* **78**, 6812–8

19. Anders, S., and Huber, W. (2010) Differential expression analysis for sequence count data. *Genome Biol.* **11**, R106

20. Edgar, R., Domrachev, M., and Lash, A. E. (2002) Gene Expression Omnibus: NCBI gene expression and hybridization array data repository. *Nucleic Acids Res.* **30**, 207–210

21. Rühl, M., Rupp, B., Nöh, K., Wiechert, W., Sauer, U., and Zamboni, N. (2012) Collisional fragmentation of central carbon metabolites in LC-MS/MS increases precision of ^{13}C metabolic flux analysis. *Biotechnol. Bioeng.* **109**, 763–771

22. Weitzel, M., Nöh, K., Dalman, T., Niedenführ, S., Stute, B., and Wiechert, W. (2013) 13CFLUX2-high-performance software suite for ^{13}C-metabolic flux analysis. *Bioinformatics* **29**, 143–5

23. Schwender, J., Shachar-Hill, Y., and Ohlrogge, J. B. (2006) Mitochondrial metabolism in developing embryos of *Brassica napus*. *J. Biol. Chem.* **281**, 34040–7

24. Larimer, F. W., Chain, P., Hauser, L., Lamerdin, J., Malfatti, S., Do, L., Land, M. L., Pelletier, D. A., Beatty, J. T., Lang, A. S., Tabita, F. R., Gibson, J. L., Hanson, T. E., Bobst, C., Torres, J. L., Peres, C., Harrison, F. H., Gibson, J., and Harwood, C. S. (2004) Complete genome sequence of the metabolically versatile photosynthetic bacterium *Rhodopseudomonas palustris*. *Nat. Biotechnol.* **22**, 55–61

25. Sauer, U. (2006) Metabolic networks in motion: ^{13}C-based flux analysis. *Mol. Syst. Biol.* **2**, 62

26. Vincenzini, M., Marchini, A., Ena, A., and De Philippis, R. (1997) H2 and poly-β-hydroxybutyrate, two alternative chemicals from purple non sulfur bacteria. *Biotechnol. Lett.* **19**, 759–762

27. Mukhopadhyay, M., Patra, A., and Paul, A. K. (2005) Production of poly(3-hydroxybutyrate) and poly(3-hydroxybutyrate-co-3-hydroxyvalerate) by *Rhodopseudomonas palustris* SP5212. *World J. Microbiol. Biotechnol.* **21**, 765–769

28. De Philippis, R. (1992) Factors affecting poly-β-hydroxybutyrate accumulation in cyanobacteria and in purple non-sulfur bacteria. *FEMS Microbiol. Lett.* **103**, 187–194

29. Anderson, A. J., and Dawes, E. A. (1990) Occurrence, metabolism, metabolic role, and industrial uses of bacterial polyhydroxyalkanoates. *Microbiol. Rev.* **54**, 450–72

30. Melnicki, M. R., Eroglu, E., and Melis, A. (2009) Changes in hydrogen production and polymer accumulation upon sulfur-deprivation in purple photosynthetic bacteria. *Int. J. Hydrog. Energy* **34**, 6157–6170

31. Cronan, J. (2002) Phospholipid modifications in bacteria. *Curr. Opin. Microbiol.* **5**, 202–205

32. Nam, T.-W., Ziegelhoffer, E. C., Lemke, R. A. S., and Donohue, T. J. (2013) Proteins needed to activate a transcriptional response to the reactive oxygen species singlet oxygen. *MBio* **4**, 10.1128/mBio.00541–12

33. Fischer, E., and Sauer, U. (2003) A novel metabolic cycle catalyzes glucose oxidation and anaplerosis in hungry *Escherichia coli*. *J. Biol. Chem.* **278**, 46446–51

34. Wendisch, V. F., de Graaf, A. A., Sahm, H., and Eikmanns, B. J. (2000) Quantitative determination of metabolic fluxes during coutilization of two carbon sources: comparative analyses with *Corynebacterium glutamicum* during growth on acetate and/or glucose. *J. Bacteriol.* **182**, 3088–96

35. Zhao, J., and Shimizu, K. (2003) Metabolic flux analysis of *Escherichia coli* K12 grown on ^{13}C-labeled acetate and glucose using GC-MS and powerful flux calculation method. *J. Biotechnol.* **101**, 101–17

36. Tang, Y. J., Chakraborty, R., Martín, H. G., Chu, J., Hazen, T. C., and Keasling, J. D. (2007) Flux analysis of central metabolic pathways in *Geobacter metallireducens* during reduction of soluble Fe(III)-nitrilotriacetic acid. *Appl. Environ. Microbiol.* **73**, 3859–64

37. Rühl, M., Le Coq, D., Aymerich, S., and Sauer, U. (2012) ^{13}C-flux analysis reveals NADPH-balancing transhydrogenation cycles in stationary phase of nitrogen-starving *Bacillus subtilis*. *J. Biol. Chem.* **287**, 27959–70

38. Ishii, N., Nakahigashi, K., Baba, T., Robert, M., Soga, T., Kanai, A., Hirasawa, T., Naba, M., Hirai, K., Hoque, A., Ho, P. Y., Kakazu, Y., Sugawara, K., Igarashi, S., Harada, S., Masuda, T., Sugiyama, N., Togashi, T., Hasegawa, M., Takai, Y., Yugi, K., Arakawa, K., Iwata, N., Toya, Y., Nakayama, Y., Nishioka, T., Shimizu, K., Mori, H., and Tomita, M. (2007) Multiple high-throughput analyses monitor the response of *E. coli* to perturbations. *Science* **316**, 593–7

39. Kranz, R., Gabbert, K., Locke, T., and Madigan, M. (1997) Polyhydroxyalkanoate production in *Rhodobacter capsulatus*: genes, mutants, expression, and physiology. *Appl. Envir. Microbiol.* **63**, 3003–3009

40. Lebedeva, N. V, Malinina, N. V, and Ivanovskiĭ, R. N. [A comparative study of the isocitrate dehydrogenases of *Chlorobium limicola forma Chlorobium thiosulfatophilum* and *Rhodopseudomonas palustris*]. *Mikrobiologiia* **71**, 762–7

41. Tahama, H., Shinoyama, H., Ando, A., and Fujii, T. (1990) Purification and characterization of isocitrate lyase from *Rhodopseudomonas* sp. No.7. *Agric. Biol. Chem.* **54**, 3177–3183

42. Singh, S. K., Matsuno, K., LaPorte, D. C., and Banaszak, L. J. (2001) Crystal structure of *Bacillus subtilis* isocitrate dehydrogenase at 1.55 A. Insights into the nature of substrate specificity exhibited by *Escherichia coli* isocitrate dehydrogenase kinase/phosphatase. *J. Biol. Chem.* **276**, 26154–63

43. Jones, S. E., and Lennon, J. T. (2010) Dormancy contributes to the maintenance of microbial diversity. *Proc. Natl. Acad. Sci. U. S. A.* **107**, 5881–6

ACKNOWLEDGEMENTS. Experimental aspects of this research were supported equally by the Division of Chemical Sciences, Geosciences, and Biosciences, Office of Basic Energy Sciences, U.S. Department of Energy (DOE), through grant DE-FG02-05ER15707 and by the Office of Science (BER), U.S. Department of Energy, through grant DE-FG02-07ER64482. Experimental work was also funded through the European Commission 7th Framework project BaSysBio (LSHG-CT-2006-037469). US National Science Foundation grant MCB-11457304 to CSH and Office of Science (BER), U.S. Department of Energy grant DE-SC0008131 to JBM provided support for data analysis and manuscript preparation. We thank Colin Lappala for assistance with RNA purification and RNAseq analysis. We also thank Dr. Amy Schaefer and other members of the Harwood lab for fruitful discussions.

FOOTNOTES

Abbreviations: acetate (Ace), acetyl-CoA (AcCoA), 1,3-bisphosphoglycerate (BPG), citrate/isocitrate (Cit/Ict), dry cell weight (DCW), α-ketoglutartate (αKG), erythrose-4-phosphate (E4P), fructose-1,6-bisphosphate (FBP), fructose-6-phosphate (F6P), glucose-6-phosphate (G6P), glyceraldehyde-3-phosphate (GAP), hydrogen gas (H_2), malate (MAL), malate dehydrogenase (malDH), malic enzyme (malic enz.), mass isotopomer distribution (MID), oxaloacetate (OAA), pentose-5-phosphate (R5P), phosphoenolpyruvate (PEP), phosphoenolpyruvate carboxykinase (PEPCK), phosphoenolpyruvate carboxylase (PEPC), phosphoenolpyruvate synthetase (PEP syn), 6-phosphogluconate (PG6), 3-phosphoglycerate (3PG), polyhydroxybutyrate (PHB), pyruvate (PYR), ribulose-1,5-bisphosphate (R1,5P), sedoheptulose-7-phosphate (S7P), succinate (SUC), tricarboxylic acid (TCA)

FIGURE LEGENDS

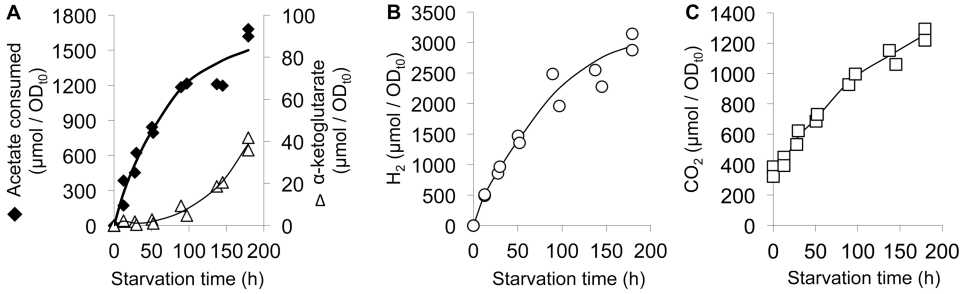

FIGURE 1. H_2 and CO_2 production and acetate consumption was rapid during the first 50-100h of nitrogen starvation and then slowed as αKG was excreted. Each data point is representative of a single sacrificed culture. Units are total µmoles normalized for the OD_{660} at the onset of nitrogen starvation to account for differences in cell density between cell suspensions.

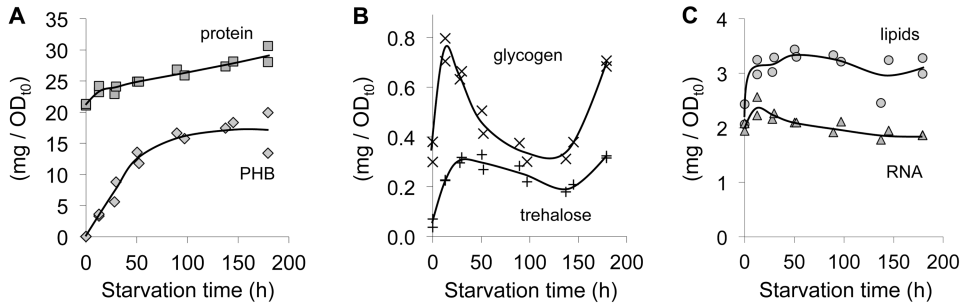

FIGURE 2. Polyhydroxybutyrate is synthesized in response to nitrogen starvation. Each data point is representative of a single sacrificed culture. Units are total mg normalized for the OD_{660} at the onset of nitrogen starvation to account for differences in cell density between cell suspensions.

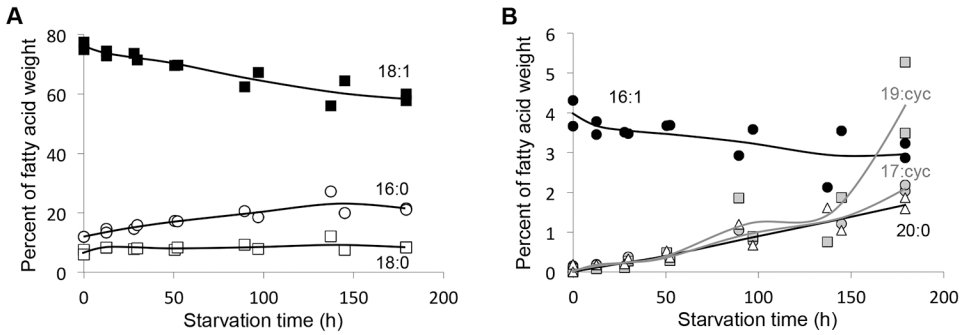

FIGURE 3. Fatty acid composition changes in favor of unsaturated fatty acids and cyclopropane fatty acids in response to nitrogen starvation. Each data point is representative of a single sacrificed culture.

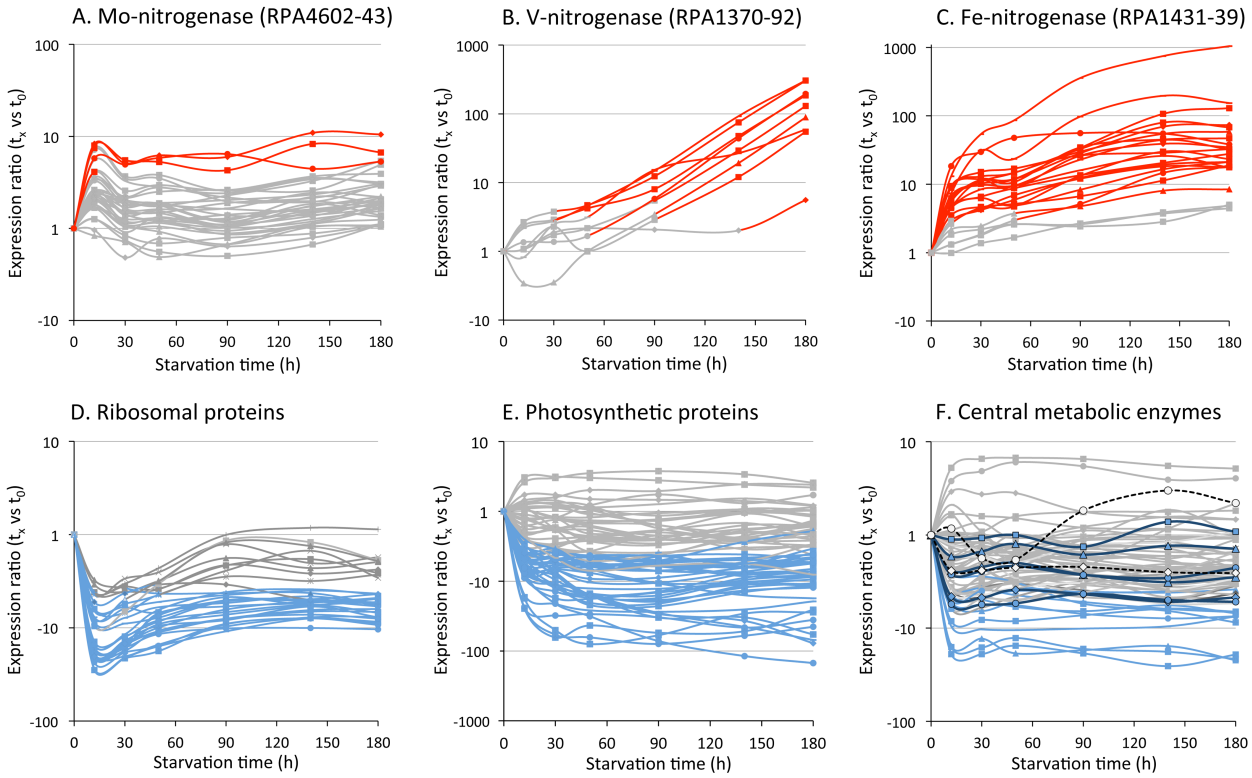

FIGURE 4. Transcript levels for genes encoding alternative nitrogenases (A-C) increased in response to nitrogen starvation while most genes for core physiological processes, such as those encoding ribosomal proteins (D), photosynthetic proteins (E), and central metabolic enzymes (F) showed lower transcript levels or no change. Genes encoding lower TCA cycle enzymes isocitrate dehydrogenase (RPA3834), αKG dehydrogenase (RPA0185-90), and succinyl-CoA synthetase (RPA0190-1) are shown as black-outlined symbols with dark blue lines. Genes encoding glyoxylate shunt enzymes, malate synthase (RPA4216) and isocitrate lyase (RPA4394) are shown as white symbols with black dotted lines (F). Red/Blue: ≥ 4-fold increase (Red) or decrease (Blue) in transcript level vs t_0 with *p*-value of ≤ 0.001. Gray: ≤ 4-fold change in transcript level vs t_0 or *p*-value of ≥ 0.001.

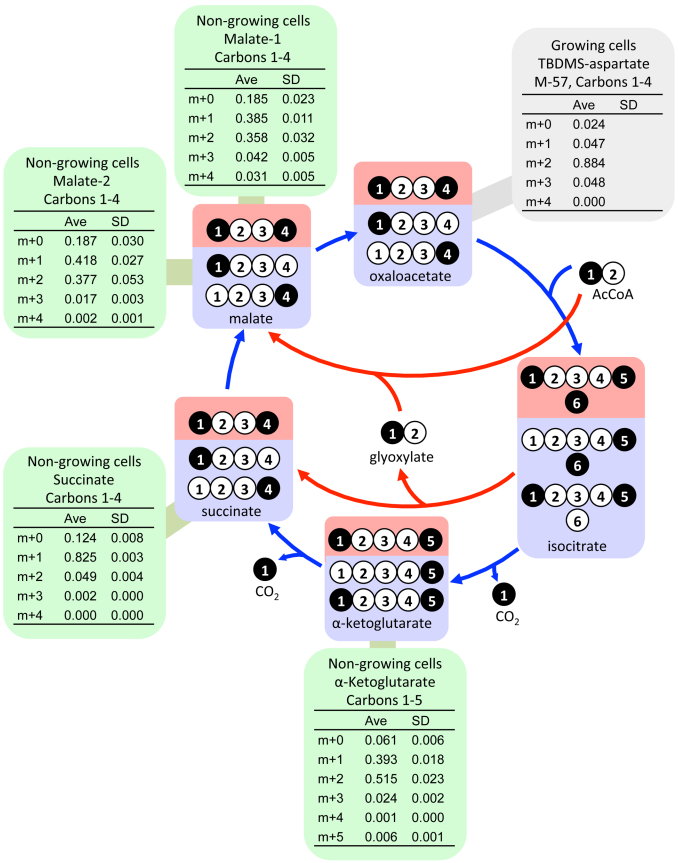

FIGURE 5. Labeling patterns that would be generated from 1-^{13}C-acetate by TCA cycle flux alone (blue) and glyoxylate cycle flux alone (red). These patterns are expected to be the dominant patterns resulting from the activity of these two cycles but can be influenced by other metabolic activities such as those shown in Figure 7. Succinate is a symmetrical molecule such that a ^{13}C-carboxyl group could represent either the first or last carbon. Green boxes show mass isotopomer distributions from metabolites from non-growing cells. αKG labeling patterns were inferred from free glutamate. The gray box shows a mass isotopomer distribution obtained from growing cells in a previous study that had near-exclusive glyoxylate shunt flux (4).

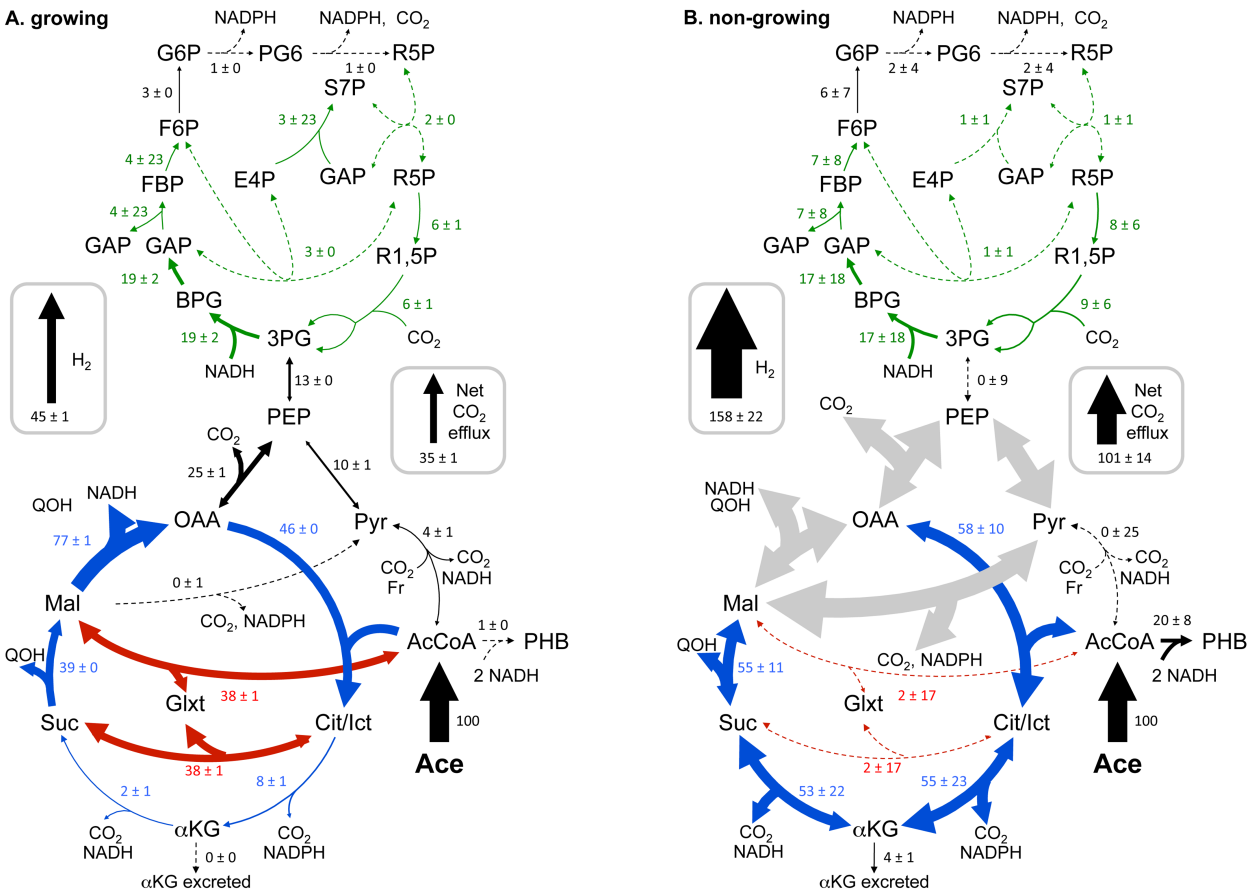

FIGURE 6. Metabolic flux distributions determined by fitting simulated mass isotopomer and extracelluar flux values to measured values using 13C-FLUX2. When growing (**A**), *R. palustris* uses the glyoxylate shunt to conserve carbon and electrons for biosynthesis. When not growing (**B**), *R. palustris* oxidizes acetate via the TCA cycle. The extra reducing power generated by the TCA cycle under non-growing conditions is coupled to H_2 production. Values for net fluxes have units of mole % of the acetate uptake rate ± SD and are reflected in arrow thickness. Dotted lines indicate values that were < 3 mole % of the acetate uptake rate. Large gray arrows indicate fluxes that could not be resolved but that best fits suggested were large in magnitude. Enlarged arrowheads indicate the direction of net flux. Actual acetate uptake rates were 0.042 ± 0.007 µmol mg DCW^{-1} h^{-1} (non-growing) and 2.0 ± 0.0 µmol mg DCW^{-1} h^{-1} (growing) (4). Unlabeled inputs of CO_2, OAA, Pyr, R5P, Suc, αKG, G6P, and AcCoA from macromolecule degradation pathways are not shown for clarity but ranged between 0 - 4 mole % of the acetate uptake rate. Data from growing cells were reported previously (4).

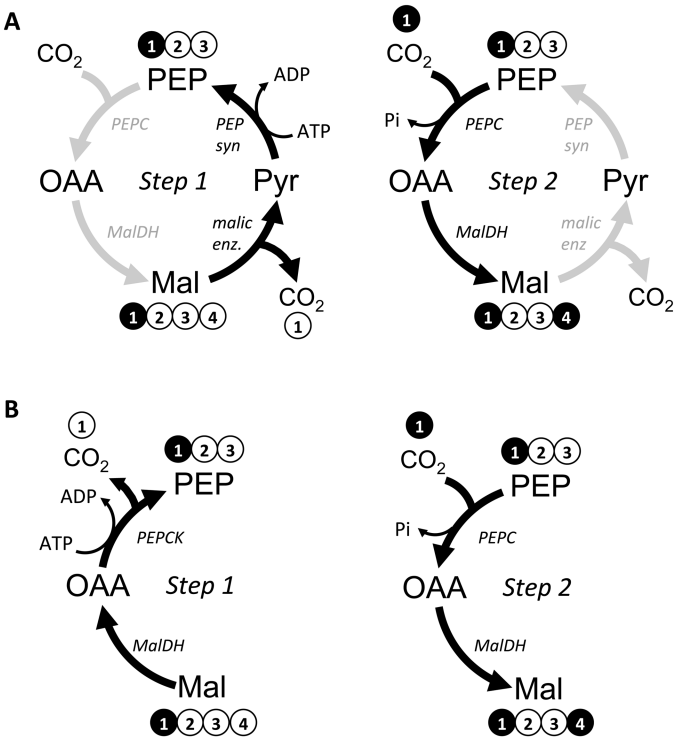

FIGURE 7. Fluxes between PEP, OAA, Mal, and Pyr are poorly resolved due to the possibility of multiple routes for generating double-labeled malate. In both **A** and **B**, single-labeled malate is decarboxylated to single labeled PEP in Step 1 but by different routes. In Step 2, PEP is carboxylated with $^{13}CO_2$ that derived from the ^{13}C-carboxyl of acetate, the main source of CO_2 in the closed system, as it is processed through decarboxylation reactions such as those in the lower TCA cycle (Fig. 4). These carboxyl exchange reactions generate double-labeled malate. These two particular scenarios represent futile cycles that result in the net expenditure of ATP. Other scenarios are possible that do not represent futile cycles, such as the reverse of the cycle depicted in panel **A**.

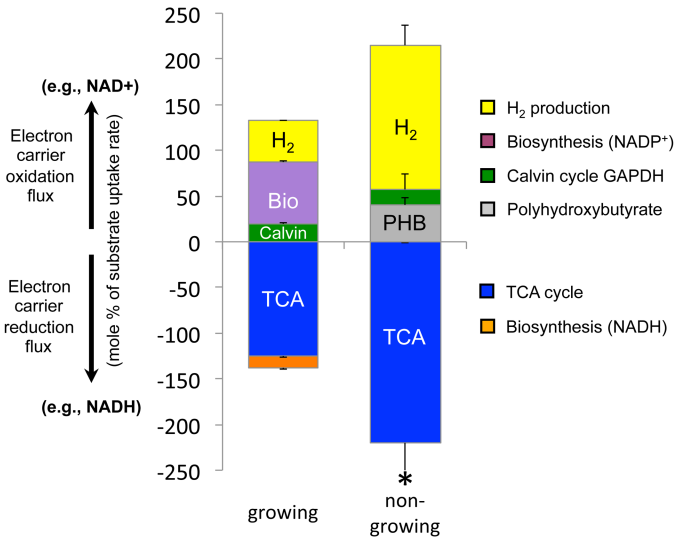

FIGURE 8. Fluxes through redox reactions are balanced under growing and non-growing conditions. Positive bars are fluxes through reactions that oxidize electron carriers whereas negative bars are fluxes through reactions that reduce electron carriers (generate reducing power). The collective bars on either side of the x-axis should be equal if electrons are balanced. The sum of oxidation reaction fluxes was 98% of the sum of reducing fluxes for growing cells and 97% for non-growing cells. Error bars represent standard deviations. * indicates that the standard deviation was larger than the mean due to participation of malate dehydrogenase in a poorly resolved cycle (Fig. 6). The contribution of malate dehydrogenase to reducing power was determined by subtracting the malic enzyme flux value from the malate dehydrogenase flux value (i.e., to determine the amount of flux needed to maintain the other flux values in the TCA cycle). The flux values for malate dehydrogenase and malic enzyme in the poorly resolved cycle were otherwise too large to make a meaningful comparison of redox fluxes. Data from growing cells were reported previously (4).